Smart Structures and Systems, *Vol. 28, No. 1 (2021) 143-152*
https://doi.org/10.12989/sss.2021.28.1.143

Study on the propagation mechanism of blast waves using the ultra-dynamic strain test system

Fei Liu [1,2], Mingzhong Gao [1,2], Ziru Guo [3], Changtai Zhou [1,2] and Jun Wang*[1,2]

[1] *Guangdong Provincial Key Laboratory of Deep Earth Sciences and Geothermal Energy Exploitation and Utilization, Shenzhen Clean Energy Research Institute, College of Civil and Transportation Engineering, Shenzhen University, Shenzhen, 518060, China*
[2] *Shenzhen Key Laboratory of Deep Underground Engineering Sciences and Green Energy, Shenzhen University, Shenzhen, 518060, China*
[3] *School of Chemical Engineering, Anhui University of Science and Technology, Huainan 232001, China*

(*Received January 19, 2021, Revised April 9, 2021, Accepted May 13, 2021*)

Abstract. The propagation mechanism of blast waves in rock materials is hard to test. This paper explores the propagation mechanism of blast-induced strain waves in coal and rock using physical modeling together with numerical modeling. The results show that the strain waves in coal blocks were weaker than that in mortar blocks under the same blast loading. With increasing distance, the strain waves induced by the shock wave show a slighter decrease in coal blocks in the radial direction, but show a stable tendency in coal blocks and a slight decrease in mortar blocks in the tangential direction. However, the strain waves induced by the explosion gas show a stable tendency in both coal and mortar blocks. The actuation duration of strain waves in coal blocks is longer than that in mortar blocks. The gap of the radial strain waves induced by shock waves is narrowed gradually and moved similarly equal to each other both in coal and mortar blocks with increasing distance. The simulated results show similar values in coal and mortar blocks as compared with the test results. The coal blocks have a better fracturing effect than that of the mortar blocks in the physical test.

Keywords: fracturing effect; strain waves; test system; ultra-dynamic

1. Introduction

Blast technology has been widely employed in exploitation of natural resource, construction of railway and tunnels, prevention of geological hazards and development and dismantling of urban buildings (Li *et al*. 2018). How to break the rocks and concrete efficiently by using the energy of explosives is vital for blasting engineering. The propagation mechanism of blast waves, including shock waves and explosion gas, and fracturing law in the internal of rock materials are of importance and is hard to test. However, it is still a challenging task for researchers to investigate the blast-induced strain waves and fractures in rock materials for its opacity. Due to the complexity of geological conditions and the construction environment, it is impossible to conduct in-situ tests. Therefore, physical models that can re-establish the conditions close to the real situation were used by previous researchers to simulate the blasting processes (Cho *et al*. 2008, Sarfarazi *et al*. 2021, Kim and Yi 2020, Choi *et al*. 2018, Kong *et al*. 2019, Cheng *et al*. 2020).

It is widely accepted that the process of blast waves is mainly consisted of shock waves and explosion gas with high temperature and pressure (Gao 2010). Due to the complexity of the process, special testing equipment and technologies are needed to measure the blast waves (Petropoulos *et al*. 2018, Rashad *et al*. 2019, Jayasinghe *et al*. 2019). Qiu (2019) employed high-speed photography to study the propagation of cracks in mode I under blast loading by caustics method. Liu (Liu *et al*. 2018) tested the explosion strain waves in mortar blocks by using the resistance strain gauges in the ultra-dynamic strain test system. The electrical measurements are most common methods for its inexpensive, repeatability and ability to test compression and tensile strain waves simultaneously.

As an alternative method, numerical modeling has become an effective method to investigate the process of blast waves with impressive results/achievements (Jean *et al*. 2019, Barla *et al*. 2012, Ajamzadeh *et al*. 2018). Shi (Shi *et al*. 2007) studied the influence of the supported mass ratio, column stiffness, the distance from the charge to the dimension, mass and geometry of the column, on the blast wave-column interaction by using AUTODYN 3D.

Based on the review of previous research, the propagation mechanism of blast-induced strain waves was investigated mainly in rock and concrete blocks. However, limited works have been carried out in coal blocks in the literature (Gary and Bailly 1998, Sarfarazi *et al*. 2018). The comparison of blast-induced strain waves in coal and rock is even not found in the literature, which has important significance and worth to have a deep study. The resistance strain gauges and ultra-dynamic systems were used to test the strain waves in coal and mortar blocks at different distances from the charge in this paper. The measured waveforms were analyzed and the propagation mechanism of blast waves in coal blocks and mortar blocks were

*Corresponding author, Ph.D.,
E-mail: junwang@szu.edu.cn

Copyright © 2021 Techno-Press, Ltd.

ISSN: 1738-1584 (Print), 1738-1991 (Online)

compared. The numerical software ANSYS/LS-DYNA with erosion criterion was used to simulate the propagation of blast-induced strain waves and fractures. The measured and simulated results are compared and included in the following sections.

2. Physical modeling and test system

2.1 Blocks preparation

The size of strain bricks was 20 mm × 20 mm × 20 mm for coal materials and 180 mm × 20 mm × 10 mm for mortar materials. The strain bricks were poured with compound materials and removed after 48 hours of curing. The coal bricks were prepared by using coal powder, cement, and water with a ratio of 2.5:2:1. Mortar bricks consisted of cement (PC32.5), sand and water with a ratio of 1:2:0.5. The resistance strain gauges were used to obtain the signals of blast waves during the explosion process. Along with the propagation of blast waves from the charge, the gauges were set in the surface of the bricks in tangential and radial directions. The strain bricks with resistance strain gauges of coal materials and mortar materials are shown as follows.

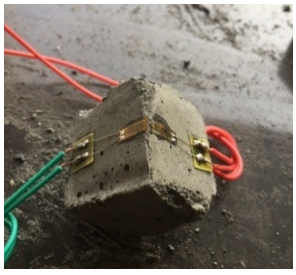

Fig. 1 Coal brick with strain gauges

Fig. 2 Coal strain brick with protective cover

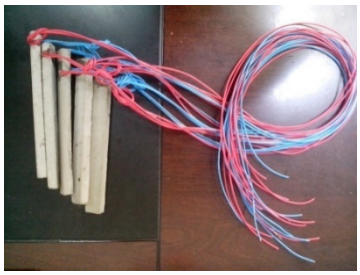

Fig. 3 Mortar strain bricks

The strain bricks with the same materials and formula were poured to make the test blocks. The compound materials were poured into a cylindrical mold with a diameter of 400 mm and a height of 400 mm for coal materials and a diameter of 400 mm and a height of 450 mm for mortar materials. First, coal materials were poured to the half-height and mortar materials were poured to 200 mm with a vibrating rod to vibrate and density the compound materials. Then, the strain bricks were installed in the materials as shown in Fig. 4 for coal block and Fig. 6 for mortar block, respectively. The embedding strain bricks for coal blocks were shown in Fig. 5 and for mortar blocks were shown in Fig. 7. The distances of the strain bricks were 50 mm, 100 mm and 150 mm from the center of the charge. The strain bricks were inserted 80 mm into the first layer in mortar blocks. The designed diagrams and first layer poured were shown as follows.

After that, the second layer of the compound materials was poured slowly into the mold to reach its top with appropriate applied vibration. A steel rod with a diameter of

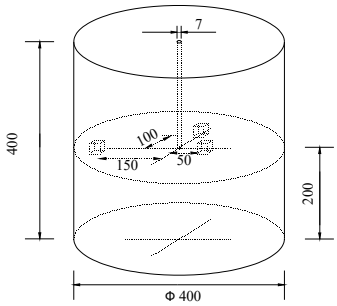

Fig. 4 The designed model for coal blocks (unit mm)

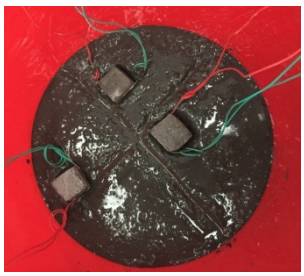

Fig. 5 Location of the embedded strain bricks in the coal blocks

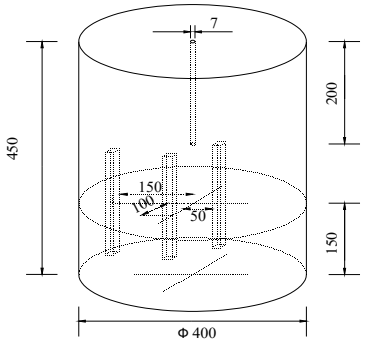

Fig. 6 The designed model for mortar blocks (unit mm)

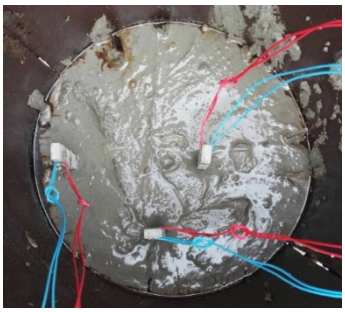

Fig. 7 Location of the embedded strain bricks in the mortar blocks

7 mm was located in the center of the mold to form a borehole, see Figs. 4 and 6. Three sets of the blocks were poured and cured with 28 days for the test of blast-induced strain waves.

2.2 Mechanical and physical parameters tests

A series of small-scale tests on the cubic coal and mortar blocks (150 mm × 150 mm × 150 mm) are carried out to derive the mechanical properties of coal and mortar materials. The compound materials used in above-section were poured into the cubic molds. The mechanical properties of the compound blocks were obtained by using uniaxial compression tests and our previous theory calculations (Liu *et al*. 2018). The P-wave velocities of the coal and mortar blocks were tested by using a CTS-25 non-metallic ultrasonic detector as shown in Fig. 8. The elastic modulus and compressive strength of the blocks were measured by using the DH3816 static strain test system and the CSS-YAW3000 electro-hydraulic servo pressure frame and the stress strain curve of mortar block was shown in Fig. 9.

Fig. 8 Test of P-wave in mortar block

Due to the Poisson's ratio μ and the shear wave velocity C_s cannot be measured directly, the elastic relationships of them can be used to calculate the results as follows.

$$C_p = \sqrt{\frac{E(1-\mu)}{\rho(1+\mu)(1-2\mu)}} \tag{1}$$

$$C_s = \sqrt{\frac{E}{2\rho(1+\mu)}} \tag{2}$$

where C_p is the velocity of longitudinal wave, E is the elastic modulus, μ is the Poisson's ratio, ρ is the density, C_s is the velocity of transverse wave.

The measured data from the three sets of mortar cubic blocks and three sets of coal cubic blocks were averaged. The measured and calculated mechanical parameters of the coal and mortar blocks are summarized in Table 1.

2.3 Test system

The test system consists of a ultra-dynamic strain test system, dynamic data-acquisition system, and some magnetic shielding circuit which can filter noise signal during the process of the test, see Fig. 10. The 120 Ω

(a) Testing instrument

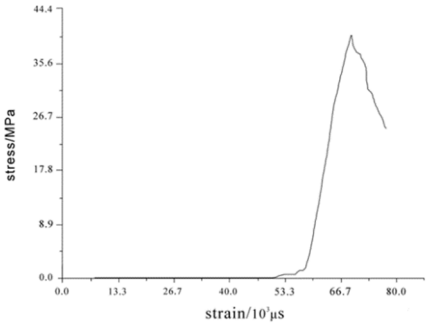

(b) stress strain curve

Fig. 9 Compressive test of mortar blocks

Table 1 Mechanical and physical parameters for compound coal and mortar materials

Blocks	Ratio C : C : W	Density ρ [g.cm^{-3}]	Compressive strength f_c [MPa]	Elastic modulus E [GPa]	Poisson's ratio μ	Velocity of longitudinal wave C_p [m.s^{-1}]	Velocity of transverse wave C_s [m.s^{-1}]
coal	2.5 : 2 : 1	1.33	9.4	36.2	0.3	6053	2916
mortar	1 : 2 : 0.5	2.1	40.05	29.30	0.28	4231	2339

Table 2 Parameters of the strain test system

Channels	Resistance of bridge [Ω]	Voltage of bridge [V]	Factor of strain K	Range of balance	Methods of balance
8	60～5 k	2/4/8	2	±3%	automatic
Resistance input [MΩ]	Sensitivity [V/με]	Multiple of increase	Noise ratio [dB]	Work temperature [℃]	Voltage output [V]
> 100	0.1/100	10/30/100/300/1000	> 40	0～40	± 5

(a) Front view

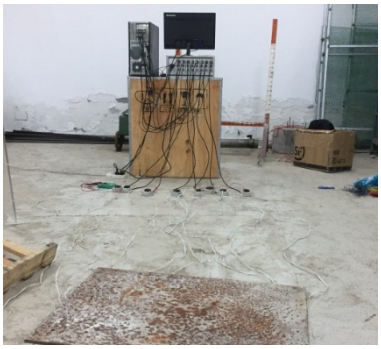

(b) Back view

Fig. 10 The ultra-dynamic strain test system for coal blocks

resistance strain gauges with the sensitive grid of 2.0 mm × 4.0 mm, the substrate of 3.5 mm × 6.5 mm and the sensitivity coefficient of 2.08 ± 0.01 are used in the test. A frequency response of DC-2500 KHz (-3 dB) with the function of compensation and automatic correction is integrated in the test system. The corresponding parameters of the test system are summarized in Table 2.

Physical experiments of the coal and mortar blocks are shown as Fig. 10. The external power supply was turned off temporarily during the testing.

The protective plate is removed and the boundary of the block is uncovered to measure reflected tensile waves on the free surface. The shielded cable is used in the test system to remove the interference of the external electromagnetic circumstance. To reduce the interference of the current, the traverse lines (10 m long) are used and the grounding wires are earthed.

3. Measured results and analysis

3.1 Signal transformation

The charge used in current study is a number 8 Nonel detonator to avoid the interference of electronic noise. The amount of explosive uses was 0.6 g RDX with a detonation velocity of 8700 m/s. The measured data are compared and the best waveform is used for analysis. The measured strain waves for the tangential direction in coal blocks and radial direction in mortar blocks at 100 mm from the borehole are lost as the channel No. 2 was broken. For the characteristic of the resistance strain gauges, the measured data are voltage signals, which can be converted to strain signals by using Eq. (3) as follows

$$\varepsilon_d = \frac{4U_o}{KU_1A} \tag{3}$$

where ε_d is the dynamic strain, K is the sensitivity coefficient, U_1 is the voltage of bridge (V), U_o is the voltage of output (V), A is the gain (100).

3.2 Analysis of strain waves

The measured strain waveforms in different directions of coal and mortar blocks are plotted in Figs. 11 and 12. As shown in Figs. 11 and 12, the radial strain wave is shown as a positive signal and the tangential strain wave is shown as a negative signal. Due to the directions of the coal strain bricks are hard to fix, the direction of the measured waveforms is not standard. The direction of strain waves in coal is changed to have a better analysis as compared to the mortar blocks. All signals are not filtered and the waveforms are shown as follows.

As shown in Figs. 11 and 12, the blast-induced strain wave has a larger peak that follows a small peak of the waveform. It is known that the process of the explosion is consisted of explosion gas and strain waves according to previous research (Rahmani *et al*. 2020). The first small peaks are negative in all the radial strain waves and positive in all the tangential strain waves. It may lie in that the compression of strain waves in radial direction and tension of strain waves in the tangential direction. However, the larger peak following the small peak is positive in both radial and tangential directions. That is due to the sudden leak of explosion gas and the reflected tensile waves appeared in the cracks.

The peaks of the waveforms in coal blocks are smaller than that in the mortar blocks, which means that the explosion waves cause a smaller strain in coal than that in mortar. The peaks of strain waves in coal blocks are gentle and have no sharp peak compared with that in mortar blocks. The actuation duration of both shock waves and explosion gas in coal blocks is longer than that in mortar

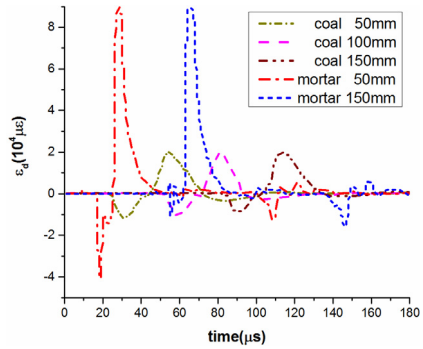

Fig. 11 Radial strain waves of coal and mortar blocks

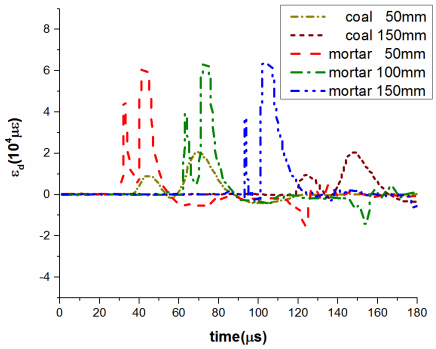

Fig. 12 Tangential strain waves of coal and mortar blocks

blocks. This is due to the coal materials have a smaller elastic modulus than that of mortar, which can slow down the propagation of shock waves and explosion gas in coal blocks.

In detail, the peak of first shock wave shows a slight decrease in coal blocks but a larger decrease in mortar blocks in the radial direction from 50 mm to 150 mm. However, the larger peak caused by the explosion gas shows a stable and unchanged tendency in both coal and mortar blocks in the radial direction. In the tangential direction, the peak of shock wave shows a stable tendency in coal blocks and a slight decrease in mortar blocks from 50 mm to 150 mm. And the peak caused by explosion gas shows an unchanged tendency in both coal and mortar blocks. In general, the mortar blocks have a stronger hindrance to the propagation of strain waves caused by shock waves than that in coal blocks. And they both have no obvious hindrance on the propagation of strain waves caused by explosion gas.

As shown in Fig. 11, the actuation duration of shock waves has a small decrease from about 20 μs at 50 mm to 16 μs at 150 mm in the radial direction in coal blocks. And it has a similar tendency from about 10 μs at 50 mm to 8 μs at 150 mm in the mortar blocks. The actuation duration of explosion gas is about 30 μs in different points and almost invariable in coal blocks. However, it has a decreased tendency from 25 μs at 50 mm to 20 μs at 150 mm in mortar blocks. As shown in Fig. 12, the actuation duration of strain waves is about 15 μs in different points and almost unchangeable in coal blocks in the tangential direction. But it has an obvious decrease from about 12 μs at 50 mm to 3 μs at 150 mm in mortar blocks. The actuation duration of explosion gas almost keeps the same as about 26 μs in different points in coal blocks, but it has an increasing tendency from about 15 μs at 50 mm to 22 μs at 150 mm in mortar blocks.

The detailed peak values of the strain waves in coal and mortar blocks are compared and the test results are shown as Table 3.

As shown in Table 3, the peak values of the strain waves caused by shock waves and explosion gas in coal and mortar blocks at both radial and tangential directions are listed except for some missing points. A detailed analysis is included as follows.

For radial strain waves, as they were caused by shock waves, the initial absolute peak value of strain waves was 1.2×10^4 με in coal block and far less than that in mortar block (4.1×10^4 με) at the distance of 50 mm. With increasing distance, the gap is narrowing (0.8×10^4 με in coal block and 1.1×10^4 με in mortar block at the distance of 150 mm). This is because the strain waves attenuated to elastic vibrational waves gradually and have a less energy attenuation with increasing distance. However, as the radial strain waves were caused by explosion gas, the gap of peak values at the same point was almost unchanged with increasing distance (2.0×10^4 με in coal block and 9.0×10^4 με in mortar block at the distance of 50 mm and that was 2.0×10^4 με and 8.9×10^4 με in coal and mortar blocks respectively at the distance of 150 mm). That is because the explosion gas can fill with the cracks instantly and will not be affected by the distance.

Table 3 Peak of strain waves

Test results				Distance from explosive [mm]		
				50	100	150
Peak value of strain wave [10^4 με]	Radial	Shock wave	Coal	-1.2	-1.0	-0.8
			Mortar	-4.1	—	-1.1
		Explosion gas	Coal	2.0	2.0	2.0
			Mortar	9.0	—	8.9
	Tangential	Shock wave	Coal	0.9	—	1.0
			Mortar	4.6	3.9	3.7
		Explosion gas	Coal	2.2	—	2.3
			Mortar	6.1	6.4	6.6

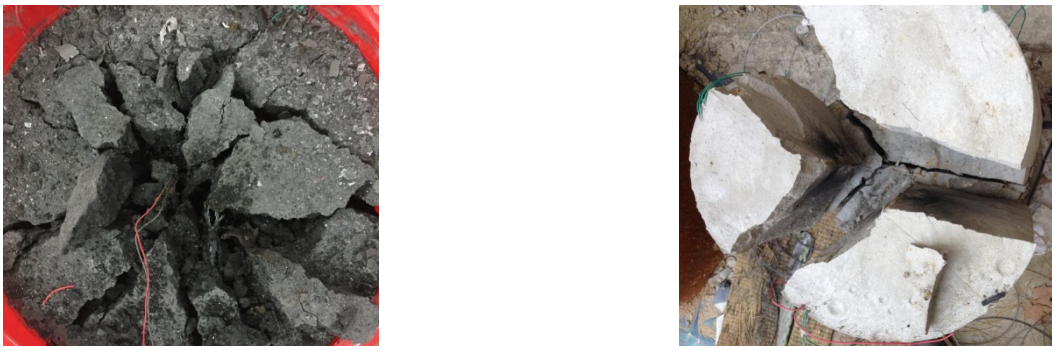

(a) Coal block (b) Mortar block

Fig. 13 Explosion effects

For tangential strain waves, as they were caused by shock waves, the absolute peak value of strain waves was 0.9×10^4 με in coal block and far less than that in mortar block (4.6×10^4 με) at the distance of 50 mm. With increasing distance, the gap is narrowing (1.0×10^4 με in coal block and 3.7×10^4 με in mortar block at the distance of 150 mm). When it comes to the strain waves caused by explosion gas, the gap of peak values widened with increasing distance (2.2×10^4 με vs. 6.1×10^4 με at the distance of 50 mm and 2.3×10^4 με vs. 6.6×10^4 με at the distance of 150 mm). That is because the tangential strain waves have a small decrease with increasing distance.

3.3 Explosion effects

The final fracturing fragment after explosion of coal and mortar are shown in Fig. 13.

It can be seen from Fig. 13 that the two blocks are both broken into many fragments. The coal block is broken sufficient with more fragments compared with the mortar block (six huge fragments). It may lie in that the coal block has a weak tensile strength than the mortar block. As is shown in Fig. 13(a), the fragments around the borehole are thrown out from the internal of the coal block and formed an explosion crater. However, the mortar block is only broken into six huge fragments and some small fragments with no explosion crater. It may due to the tensile strength of the mortar materials is greater and the energy of the explosive can hardly break it into small pieces.

4. Numerical simulations

4.1 General considerations

Numerical simulation is also an effective way to analyze this complex problem (Nelson and O'Toole 2018). The propagation mechanism of explosion strain waves and cracks in coal blocks and mortar blocks are compared by using ANSYS/LS-DYNA numerical analysis. The dimensions of explosive, stemming, coal and rock are modeled in the simulation models according to the test blocks as shown in Figs. 4 and 6. The model as simplified into a single-layer solid grid model for modeling and calculating facilitated (Shi *et al*. 2005). The free surface at the top, bottom and both sides of the model are set for closer to the physical models. The Arbitrary Lagrangian-Eulerian (ALE) in the finite element method (FEM) and fluid-solid coupling algorithm are used to make connections between the two materials, so that substances can flow in the grid to avoid severe structural distortions of the elements. The mechanical parameters of coal and mortar materials from Table 1 are used for numerical modeling. Note that the quasistatic properties of coal and mortar materials were used for numerical simulation for simplification. The material properties of stemming, coal and mortar are implemented in the model following the procedures of the LS-DYNA keyword user's manual (LSTC 2003).

4.2 Explosive and Equation of State (EOS)

In this paper, the RDX is used as the high-energy explosive with the parameters as follows: Density is 1630 Kg•m^{-3}; Chapman-Jouget pressure is 2.7 GPa; Detonation velocity is 6930 m•s^{-1}. The JWL equation of state (EOS), proposed by Jones-Wilkens-Lee, is used to represent material parameters of explosive material which related the pressure to the specific volume generated by the process of detonation (Lee *et al*. 1968). It has been widely used in blasting calculations and can be written as

$$P = A\left(1 - \frac{\omega}{R_1 V}\right)e^{-R_1 V} + B\left(1 - \frac{\omega}{R_2 V}\right)e^{-R_2 V} + \frac{\omega E_0}{V} \quad (4)$$

where E_0 is the initial specific internal energy, 7.0 MJ; P is pressure in MPa; V is the relative volume of initial, 1.0; the characteristic parameters of the material as R_1, R_2, A, B, and ω are 371 GPa, 7.43 GPa, 4.15, 0.95, and 0.07, respectively.

4.3 Stemming properties

The Plastic-Kinematic type is used as the constitutive behavior for coal and rock which can be used to model the strain-rate effects of kinematic hardening plasticity. The parameters for the two materials can be obtained from the test results of the standard blocks. The von Misses type and the keyword *MAT_SOIL_AND_FOAM with elastic-plastic behavior are used to model the stemming material. The parameters are summarized in Table 4 (Bai 2005).

Table 4 Material parameters of stemming (Bai 2005)

Density/ρ_0 ($g \cdot cm^{-3}$)	Shear modulus/G (GPa)	Bulk modulus/K (GPa)	A_0	A_1	A_2	P_C(KN)	EPS_1	EPS_2
1.80	1.601E-4	1.328E+2	3.3E-3	1.31E-7	0.1232	0.0	0.0	0.05
EPS_3	EPS_4	EPS_5	EPS_6	EPS_7	EPS_8	EPS_9	EPS_{10}	P_1
0.09	0.11	0.15	0.19	0.21	0.22	0.25	0.30	0.0
P_2	P_3	P_4	P_5	P_6	P_7	P_8	P_9	P_{10}
3.42E-2	0.453	0.676	0.127	0.208	0.271	0.392	0.566	1.23

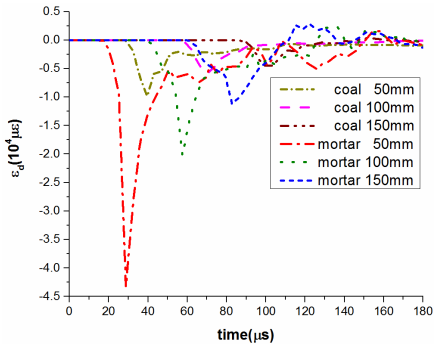

Fig. 14 Radial strain waves for coal and mortar blocks

Note, A_0~A_2 are constant of yield function corresponding to plastic yield, EPS_1~EPS_{10} are volumetric strain values (natural logarithmic values), and P_1~P_{10} are volumetric strain values which corresponded to pressures, in KN.

4.4 Simulated results and analysis

The coal model and mortar model are calculated respectively. The strain waves at 50 mm, 100 mm, and 150 mm from the charge in coal block and mortar block are extracted out and compared. As the models are single-layer solid grid and the software cannot simulate the propagation of explosion gas as it enters into the cracks and makes the tensile fractures, the strain waves caused by explosion gas are not obtained. The strain waves generated by the shock wave in coal and mortar blocks are shown as Fig. 14.

As shown in Fig. 14, the radial strain waves in coal blocks are far weaker than that in mortar blocks. Compared with the test results, the strain waves of numerical results at different points in the two types of blocks also have a decline trendy with increasing distance. In details, the absolute peak values of strain waves in coal blocks have a slight decline trend from about 1.0×10^4 με at 50 mm to 0.5×10^4 με at 150 mm. It is consistent with the physical test result. However, the absolute peak values of strain waves in mortar blocks have a large decline trend from about 4.3×10^4 με at 50 mm to 1.2×10^4 με at 150 mm. They also have similar values compared to the test results, which show that the test results are reliable.

An erosion criterion was used in these models to simulate the propagation of fractures under explosion loading. The elements of explosives are removed to have a better view of the broken effects on the coal and mortar blocks. The final crushing effects of coal and mortar blocks are shown as Fig. 15.

As seen from Fig. 15, many cracks are created in both of the two models. The explosion cavity appeared around the charge in both of them which was caused by the compression effects of an intense impact. At the corners of the models, a large number of cracks are concerned and shown on the diagonal angle, which is due to the compress strain waves propagated to the free surface at the corners and the reflection effect appeared. Then the compress strain waves are converted into reflected tensile waves and observed on the diagonal angle to have the tensile fractures. The coal and mortar materials can be broken easily by tensile waves as they have a weak property of tensile strength.

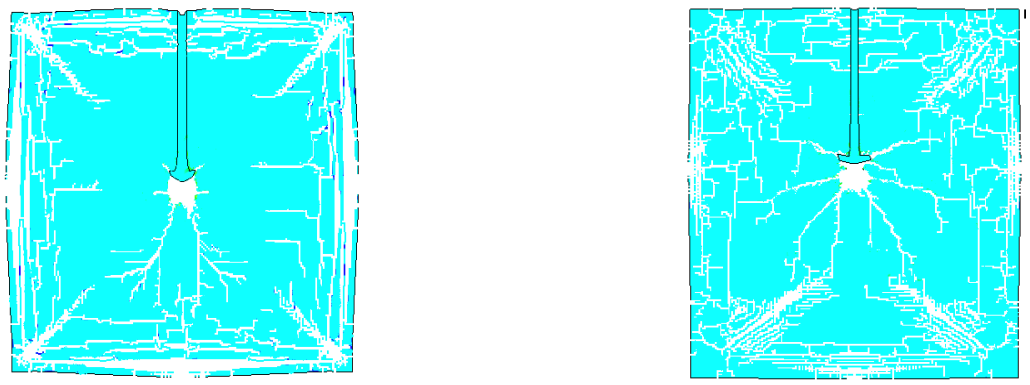

(a) Coal block (b) Mortar block

Fig. 15 Final crushing effects of the coal and mortar blocks

The coal block has concentrated fractures, but the mortar block has more dispersive fractures. In detail, more cracks appeared around the boundary of the coal block than that in the mortar block. And fewer cracks appeared in the center zone of the coal block than that in the mortar block. That is because the explosive used with a high detonation velocity, which can make compression fractures easily in the materials with high compress strength. The induced blast waves break the boundary of coal blocks into persistent fractures, resulting more small fragments, while more small local fractures are formed in mortar materials, leading to large fragments. Therefore, the simulation results are consistent with experimental observations in Section 3.3.

5. Comparison of measured and simulated results

The radial and tangential strain waves in coal and mortar blocks were compared and discussed by using test and numerical methods. The validation of measured results on coal and mortar blocks was conducted by comparing with the simulated results. Due to the tangential strain waves cannot be obtained and the propagation of explosion gas cannot be simulated in the single-layer solid grid, the radial strain waves are modified and the measured and simulated results in coal and rock blocks are compared in Figs. 16 and 17.

As shown in Figs. 16 and 17, the simulated results have a similar tendency with the measured results in both coal and mortar blocks. As shown in Fig. 16, the radial strain waves at the distance of 50 mm, 100 mm and 150 mm from the charge in coal blocks are measured in physical models and simulated in numerical models. The peak values of simulated strain waves are slightly greater and lager than that of the measured results at all test points, which may due to the block of bedding planes and cracks in physical models. However, the simulated strain waves in mortar blocks have a good similar tendency with that of the measured results, see Fig. 17. It indicates that the measured and the simulated results are reliable.

6. Conclusions

The blast-induced strain waves and fractures in coal and mortar blocks were compared by using physical modeling and numerical calculations. Some conclusions were summarized as follows.

The coal blocks have a smaller strain effect than mortar blocks under the same blast loading. The peaks of strain waves in mortar blocks were sharper than those in the coal blocks. The actuation duration of the shock waves and explosion gas in coal blocks were all longer than that in mortar blocks. The actuation duration of shock wave and explosion gas was shown as a small decrease tendency in both coal and mortar blocks with increasing distance, except for that of explosion gas is invariable in coal blocks in the radial direction. In the tangential direction, the actuation duration of both shock waves and explosion gas in coal blocks almost kept the same. However, that of shock waves showed obviously decrease and that of explosion gas shows a small increase tendency in mortar blocks.

In the radial direction, the strain waves caused by the shock wave showed a slighter decrease in coal blocks than that in mortar block with increasing distance. However, the strain waves caused by the explosion gas showed a stable and unchanged tendency in both coal and mortar blocks. In the tangential direction, the peak of strain waves caused by shock wave showed a stable tendency in coal blocks and a slight decrease in mortar blocks with increasing distance. And that caused by explosion gas showed an unchanged tendency in both coal and mortar blocks.

With increasing distance, the gap of the radial strain waves induced by shock waves was narrowed gradually and moved similarly equal to each other both in coal and mortar blocks. However, that induced by explosion gas were almost unchanged. The gap of the tangential strain waves induced by shock waves was narrowing but that induced by explosion gas was widening with increasing distance.

The radial strain waves caused by the shock waves showed similar values in coal and mortar blocks in numerical results as compared with test results. The fractures were concerned in coal blocks in numerical calculations, but they were more dispersive in the mortar blocks. The physical modeling tests showed that the coal block is broken into fragments with an explosion crater, but the mortar block was broken into six huge fragments with little small pieces.

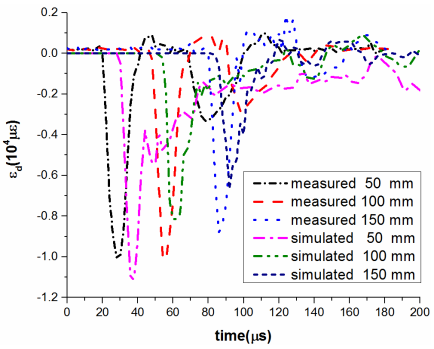

Fig. 16 Comparison of radial strain waves in coal blocks

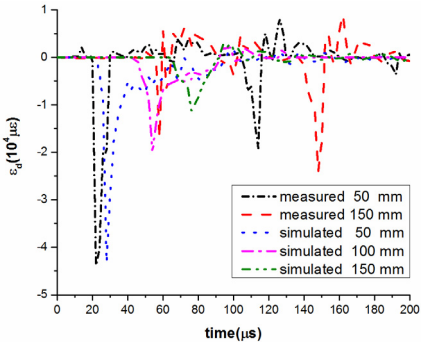

Fig. 17 Comparison of radial strain waves in mortar blocks

Acknowledgments

The authors thank the supports from National Natural Science Foundation of China (No. U19A2098, No. 51827901).

Conflict of interest

The authors declare that they have no conflict of interest.

References

Ajamzadeh, M.R., Sarfarazi, V., Haeri, H. and Dehghani, H. (2018), "The effect of micro parameters of PFC software on the model calibration", *Smart Struct. Syst.*, *Int. J.*, **22**(6), 643-662. http://dx.doi.org/10.12989/sss.2018.22.6.643

Bai, J.Z. (2005), *Theoretical Basis and Case Analysis of LSDYNA3D*, Science Press, Beijing, Beijing, China.

Barla, M., Piovano, G. and Grasselli, G. (2012), "Rock slide simulation with the combined finite-discrete element method", *Int. J. Geomech.*, **12**(6), 711-721. https://doi.org/10.1061/(asce)gm.1943-5622.0000204

Cheng, Z.B., Li, L.H. and Zhang, Y.N. (2020), "Laboratory investigation of the mechanical properties of coal-rock combined body", *Bull. Eng. Geol. Environ.*, **79**, 1947-1958. https://doi.org/10.1007/s10064-019-01613-z

Cho, S.H., Nakamura, Y. and Mohanty, B. (2008), "Numerical study of fracture plane control in laboratory-scale blasting", *Eng. Fract. Mech.*, **75**(13), 3966-3984. https://doi.org/10.1016/j.engfracmech.2008.02.007

Choi, J.H., Choi, S.J. and Kim, J.H.J. (2018), "Evaluation of blast resistance and failure behavior of prestressed concrete under blast loading", *Constr. Build. Mater.*, **173**, 550-572. https://doi.org/10.1016/j.conbuildmat.2018.04.047

Gao, X.T. (2010), *Test on Super Dynamic Strain in Explosion Test Block*, D. Huainan: Anhui University of Science & Technology.

Gary, G. and Bailly, P. (1998), "Behaviour of quasi-brittle material at high strain rate. Experiment and modeling", *Eur. J. Mech. - A/Solids*, **17**(3), 403-420. https://doi.org/10.1016/S0997-7538(98)80052-1

Jayasinghe, B., Zhao, Z.Y., Chee, A.G.T., Zhou, H.Y. and Gui, Y.L. (2019), "Attenuation of rock blasting induced ground vibration in rock-soil interface", *J. Rock Mech. Geotech. Eng.*, **11**(4), 770-778. https://doi.org/10.1016/j.jrmge.2018.12.009

Jean, Y., Chen, G. and Gu, C. (2019), "Computational modeling and forensic analysis for terrorist airplane bombing: A case study", *Eng. Fract. Mech.*, **211**, 137-160. https://doi.org/10.1016/j.engfracmech.2019.01.032

Kim, B. and Yi, J.H. (2020), "Structural model updating of the Gageocho Ocean Research Station using mass reallocation method", *Smart Struct. Syst.*, *Int. J.*, **26**(3), 291-309. http://dx.doi.org/10.12989/sss.2020.26.3.291

Kong, D., Cheng, Z. and Zheng, S. (2019), "Study on failure mechanism and stability control measures in large-cutting-height coal mining face with deep-buried seam", *Bull. Eng. Geol. Environ.*, **78**(8), 6143-6157. https://doi.org/10.1007/s10064-019-01523-0

Lee, E.L., Hornig, H.C. and Kury, J.W. (1968), "Adiabatic expansion of high explosive detonation products", Report UCRL-50422, University of California, Lawrence Radiation Laboratory, Livermore, CA, USA.

Li, A., Fang, Q., Zhang, D.L., Luo, J.W. and Hong, X.F. (2018), "Blast vibration of a large-span high-speed railway tunnel based on microseismic monitoring", *Smart Struct. Syst.*, *Int. J.*, **21**(5), 561-569. http://dx.doi.org/10.12989/sss.2018.21.5.561

Liu, F., Guo, Z.R., Lv, H.Y. and Cheng, Z.B, (2018), "Test and analysis of blast wave in mortar test block", *Int. J. Rock Mech. Min. Sci.*, **108**, 80-85. https://doi.org/10.1016/j.ijrmms.2018.06.003

Livermore Software Technology Corporation (LSTC) (2003), LSDYNA Keyword User's Manual, Version 970. Livermore, CA, USA.

Mehdi, S.C., Ghodrat, K. and Mariusz, Z. (2009), "Numerical analysis of blast-induced wave propagation using FSI and ALEmulti-material formulations", *Int. J. Impact Eng.*, **36**(10-11), 1269-1275. https://doi.org/10.1016/j.ijimpeng.2009.03.007

Nelson, S.M. and O'Toole, B.J. (2018), "Computational analysis of blast loaded composite cylinders", *Int. J. Impact Eng.*, **119**, 26-39. https://doi.org/10.1016/j.ijimpeng.2018.04.013

Petropoulos, N., Wimmer, M. and Johansson, D. (2018), "Compaction of Confining Materials in Pillar Blast Tests", *Rock Mech. Rock Eng.*, **51**, 1907-1919. https://doi.org/10.1007/s00603-018-1447-8

Qiu, P., Yue, Z.W. and Yang, R.S. (2019), "Mode I stress intensity factors measurements in PMMA by caustics method: A comparison between low and high loading rate conditions", *Polym. Test.*, **76**, 273-285. https://doi.org/10.1016/j.polymertesting.2019.03.029

Rahmani, M., Oskouei, A.N. and Petrudi, A.M. (2020), "Experimental and numerical study of the blast wave decrease using sandwich panel by granular materials core", *Defence Technology*, In-press. https://doi.org/10.1016/j.dt.2020.09.004

Rashad, M., Wahab, M.M.A. and Yang, T.Y. (2019), "Experimental and numerical investigation of RC sandwich panels with helical springs under free air blast loads", *Steel Compos. Struct.*, *Int. J.*, **30**(3), 217-230. http://dx.doi.org/10.12989/scs.2019.30.3.217

Sarfarazi, V., Haeri, H. and Shemirani, A.B. (2018), "Simulation of fracture mechanism of pre-holed concrete model under Brazilian test using PFC3D", *Smart Struct. Syst.*, *Int. J.*, **22**(6), 675-687. http://dx.doi.org/10.12989/sss.2018.22.6.675

Sarfarazi, V., Abharian, S. and Ghorbani, A. (2021), "Physical test and PFC modelling of rock pillar failure containing two neighboring joints and one hole", *Smart Struct. Syst.*, *Int. J.*, **27**(1), 123-137. http://dx.doi.org/10.12989/sss.2021.27.1.123

Shi, D.Y., Li, Y.C. and Zhang, S.M. (2005), Display Dynamic Analysis Based on ANSYS/LS-DYNA8.1, Tsinghua University Press, Beijing, China.

Shi, Y.C., Hao, H. and Li Z.X. (2007), "Numerical simulation of blast wave interaction with structure columns", *Shock Waves*, **17**(1-2), 113-133. https://doi.org/10.1007/s00193-007-0099-5

CC

List of symbols

C_p	Velocity of longitudinal wave
E	Elastic modulus
μ	Poisson's ratio
ρ	Density
C_s	Velocity of transverse wave
ε_d	Dynamic strain
K	Sensitivity coefficient
U_1	Voltage of bridge
U_o	Voltage of output
A	Gain (100)
E_0	Initial specific internal energy
P	Pressure
V	Relative volume of initial, 1.0;
A_0~A_2	Constant of yield function corresponding to plastic yield
P_1~P_{10}	Volumetric strain values which corresponded to pressures
EPS_1~EPS_{10}	Volumetric strain values (natural logarithmic values)
R_1, R_2, A, B, ω	Characteristic parameters of the material